Cellular/Molecular

Calcium-Activated SK Channels Influence Voltage-Gated Ion Channels to Determine the Precision of Firing in Globus Pallidus Neurons

Christopher A. Deister,[1] C. Savio Chan,[2] D. James Surmeier,[2] and Charles J. Wilson[1]

[1]Department of Biology and Neurosciences Institute, University of Texas at San Antonio, San Antonio, Texas 78249, and [2]Department of Physiology and Institute for Neuroscience, Feinberg School of Medicine, Northwestern University, Chicago, Illinois 60611

Globus pallidus (GP) neurons fire rhythmically in the absence of synaptic input, suggesting that they may encode their inputs as changes in the phase of their rhythmic firing. Action potential afterhyperpolarization (AHP) enhances precision of firing by ensuring that the ion channels recover from inactivation by the same amount on each cycle. Voltage-clamp experiments in slices showed that the longest component of the GP neuron's AHP is blocked by apamin, a selective antagonist of calcium-activated SK channels. Application of 100 nM apamin also disrupted the precision of firing in perforated-patch and cell-attached recordings. SK channel blockade caused a small depolarization in spike threshold and made it more variable, but there was no reduction in the maximal rate of rise during an action potential. Thus, the firing irregularity was not caused solely by a reduction in voltage-gated Na^+ channel availability. Subthreshold voltage ramps triggered a large outward current that was sensitive to the initial holding potential and had properties similar to the A-type K^+ current in GP neurons. In numerical simulations, the availability of both Na^+ and A-type K^+ channels during autonomous firing were reduced when SK channels were removed, and a nearly equal reduction in Na^+ and K^+ subthreshold-activated ion channel availability produced a large decrease in the neuron's slope conductance near threshold. This change made the neuron more sensitive to intrinsically generated noise. *In vivo*, this change would also enhance the sensitivity of GP neurons to small synaptic inputs.

Introduction

Neurons of the external globus pallidus (GP) fire action potentials periodically, even in the absence of synaptic input (Chan et al., 2004; Hashimoto and Kita, 2006), raising the possibility that they may encode information through changes in spike time as well as changes in rate. Intrinsic variability in the firing pattern imposes a limit on the precision with which information can be encoded by spike times. Variability also limits the degree to which oscillating neurons may synchronize their firing. In healthy animals, correlations in firing of pallidal neurons have been shown to be rare or nonexistent (Nini et al., 1995; Raz et al., 2000; Stanford, 2003). However, large-scale synchrony among pallidal neurons is observed in parkinsonism (Nini et al., 1995; Raz et al., 2000; Levy et al., 2002). Synaptic inputs also introduce variability in spike timing and may disrupt synchrony to the extent that they are uncorrelated, but intrinsic variability is unique in that it is always uncorrelated among neurons, and so can never contribute to synchronous firing. For this reason, oscillating neurons may regulate their tendency to synchronize by controlling the ionic mechanisms responsible for the variability of their autonomous firing.

Subthreshold activated Na^+ current brings the neuron to threshold on each cycle of the GP cell oscillation (Mercer et al., 2007). Availability of inward current is partly determined by the depth and duration of membrane potential afterhyperpolarization. Voltage-gated K^+ channels contribute to the repolarization of the membrane potential and fast afterhyperpolarization (fAHP). The fAHP typically lasts 1–2 ms after a spike, but recovery from inactivation of the ion channels required for pacemaking requires longer periods of hyperpolarization. The longer component of the AHP referred to as the medium afterhyperpolarization (mAHP) lasts 10–20 ms, making it more likely to influence the availability of voltage-gated ion channels.

Blockade of mAHP current might be expected to increase firing rate by reducing the duration of afterhyperpolarization and the recovery of K^+ channels from inactivation. However, these may be mitigated or reversed by a decrease in Na^+ channel availability, thereby slowing the depolarizing phase of the membrane potential trajectory (Mercer et al., 2007). Thus the mAHP may not only directly control the membrane potential early in cell's oscillatory cycle, but also influence ion channels acting over later parts, long after the mAHP is complete.

We find that small-conductance Ca^{2+}-activated K^+ (SK) channels underlie most of the mAHP in GP neurons. This mAHP conductance is a small component of the overall outward current that flows during the subthreshold part of the oscillatory cycle, the majority of which is provided instead by an inactivating K^+

Received Feb. 3, 2009; revised April 28, 2009; accepted May 16, 2009.

This work was supported by National Institute of Neurological Disorders and Stroke Grant NS47085 (C.J.W., D.J.S.), Ruth L. Kirschstein National Research Service Award F31NS064755 (C.A.D.), the American Parkinson Disease Association Research Grant Program (C.S.C.), and a Parkinson's Disease Foundation International Research Grant (C.S.C.).

Correspondence should be addressed to Charles J. Wilson, Department of Biology, University of Texas at San Antonio, One UTSA Circle, San Antonio, TX 78249. E-mail: charles.wilson@utsa.edu.

DOI:10.1523/JNEUROSCI.0576-09.2009

Copyright © 2009 Society for Neuroscience 0270-6474/09/298452-10$15.00/0

current. SK channels govern the availability of voltage-gated Na^+ and K^+ channels, and so the total conductance of the cell during the approach to threshold. This change in conductance determines the sensitivity of the neuron to intrinsic channel noise and synaptic inputs, and thus indirectly controls both the sensitivity and the precision of spike time coding by GP neurons.

Materials and Methods

Animal handling and slice preparation. Both Sprague Dawley rats (Charles River) aged 15–25 d and C57BL/6 mice (Harlan) aged 17–22 d were used in this study. Animal handling and all procedures were approved by Institutional Animal Care and Use Committees and were in accordance with National Institutes of Health guidelines. All efforts to minimize both the discomfort to and the number of animals were made. Animals were anesthetized with a lethal dose of ketamine and xylazine (90 mg/ml and 10 mg/ml) and then rapidly decapitated. Brains were quickly removed and placed into ice-cold artificial CSF (ACSF) comprising the following (in mM): 126 NaCl, 2.5 KCl, 1.25 NaH_2PO_4, 26 $NaHCO_3$, 2.0 $MgSO_4$, 10 dextrose, and 2.0 $CaCl_2$ continuously bubbled with 95% O_2–5% CO_2 (carbogen). Tissue blocks containing the GP and its surrounding structures were prepared and sliced at 300 μm thickness in either the sagittal or coronal plane using a vibrating tissue slicer (Leica VT-1000s). After the initial preparation, slices were allowed to equilibrate at either 37°C for 30 min or at room temperature for 1 h, before they were used.

Electrophysiological recordings. Slices were transferred to a recording chamber that was continuously perfused with oxygenated ACSF at a rate of 2–3 ml/min. The temperature was maintained at 33–35°C for experiments when rats were used and at room temperature for experiments using mice. Infrared differential interference contrast (IR-DIC) video microscopy was used to visualize slices through a 40× water-immersion lens equipped to either a Zeiss Axioscope or an Olympus BX51 upright microscope. Patch pipettes were pulled from thin-walled borosilicate glass (outer diameter = 1.5 mm, inner diameter = 1.17 mm) using either a P-97 or P-87 Flaming-Brown electrode puller (Sutter Instruments). For cell-attached or whole-cell recordings, the electrodes were filled with a solution containing the following (in mM): 140.5 $KeMeSO_4$, 0.2 EGTA, 7.5 NaCl, 10 HEPES, 0.01 phosphocreatine, 2 NaATP, and 0.2 NaGTP, adjusted to a pH of 7.3 with KOH. The whole-cell solution was also used for perforated-patch recordings, except gramicidin-D (Sigma) was added at a final concentration of 50–100 μg/ml and sonicated 15–20 min before recording. The final tip resistance was 5–10 MΩ for both cell-attached and whole-cell recordings and 2–5 MΩ for perforated patch. For whole-cell recordings, we measured a −7 mV liquid junction potential. Recordings were made using either an Axopatch 200B or MultiClamp 700A amplifier (Molecular Devices). Signals were digitized at 10–20 kHz and low-pass filtered with a corner frequency of 5–10 kHz. Digitized data were saved for off-line analysis to a hard disk using PClamp 8.1 software (Molecular Devices). Series resistances for whole-cell recordings ranged from 2 to 5 MΩ and 10 to 60 MΩ in perforated patch. If the series resistance increased >25%, the data were discarded. A large and rapid decrease in series resistance during a perforated-patch recording was interpreted as a rupture of the patch, and the data in these cases were discarded.

Drugs. All recordings were made in the presence of 50 μM MK-801 (an NMDA receptor antagonist), 10 μM DNQX or NBQX (AMPA receptor antagonists), and 100 μM picrotoxin or 20 μM SR-95531 ($GABA_A$ receptor antagonists) to prevent spontaneous synaptic transmission, which may be present in our slice preparation, from influencing our results. All drugs were obtained from Sigma-Aldrich. SR-95531 and apamin were prepared as 1000× stocks in H_2O and diluted to achieve their final concentrations. Apamin is a selective antagonist of $K_{Ca}2.1$, 2.2, and 2.3 channels, and its ability to block is sensitive to mutations of the K_{Ca} channel pore, suggesting that it works by a direct negative interaction with the pore (Ishii et al., 1997). DNQX, NBQX, MK-801, and NS309 were prepared as 1000× stocks in DMSO; equivalent amounts of DMSO were added to control solutions.

Data analysis and statistics. Electrical traces were analyzed off-line using custom-written software, Igor Pro 5 (WaveMetrics), and Mathematica 5.2 (Wolfram Research). All statistics were performed using the software package R (R Foundation for Statistical Computing). Wilcoxon signed-rank test, for repeated measures, or a Mann–Whitney *U*, for unpaired samples, were used to evaluate whether the groups differed. A p value of <0.05 was used as our significance level for all tests. V and W are the values returned by the Wilcoxon signed-rank and Mann–Whitney U tests, respectively, which were used to calculate the p values. All numerical data are expressed as the value ± the sample-corrected SEM.

Single-cell reverse transcription-PCR. Acutely isolated mouse GP neurons were aspirated into sterilized glass pipettes containing nominally RNase-free patch solution or diethylpyrocarbonate-treated water and 0.8 U/μl SUPERase-In (Ambion). Sterile gloves were worn during the procedure to minimize RNase contamination. After aspiration, the contents of the pipette were ejected into 0.6 ml presiliconized tubes (Midwest Scientific) containing a reverse transcription (RT) mix. This mix contained 0.7 μl of SUPERase-In (20 U/μl), 1.9 μl of diethylpyrocarbonate-treated water, 1 μl of dNTPs (10 mM), 0.7 μl of BSA (143 ng/μl), and 0.7 μl of oligo-dT (0.5 μg/μl). The mixture was heated to 65°C for 5 min to denature mRNA and then placed on ice for at least 1 min. Single-strand cDNA was synthesized from the cellular mRNA by adding 2 μl of 10× PCR RT buffer, 4 μl of $MgCl_2$ (25 mM), 2 μl of DTT (0.1 M), 1 μl of RNaseOUT (40 U/μl), and 6 μl of diethylpyrocarbonate-treated water. This mixture was then incubated at 42°C for 2 min. After the initial incubation, 0.7 μl of Superscript II (50 U/μl) was added, and the mixture was kept at 42°C for an additional 50 min. The reaction was terminated by heating to 70°C for 15 min. The RNA strand in the RNA–DNA hybrid was then removed by adding 0.5 μl of RNase H (2 U/μl) and incubating at 37°C for 20 min. All reagents except SUPERase-In (Ambion) were obtained from Invitrogen. Primers and reaction protocols for parvalbumin (PV), enkephalin (ENK), and glutamic acid decarboxylase (GAD67) have been described previously (Surmeier et al., 1996; Vysokanov et al., 1998). Single-cell cDNA was amplified using a conventional PCR approach with a programmable thermal cycler (MJ Research). PCR primers were developed from GenBank sequences with commercially available OLIGO 6.7.1 software (National Biosciences). $SK1/K_{Ca}2.1$ (GenBank accession number AF116525) was detected with a pair of primers GGAGAGCCGACTGGATGTC (position 1635) and TCTAGCGGTCAGTAGCCATCAC (position 1800), which gave a PCR product of 187 bp. $SK2/K_{Ca}2.2$ (GenBank accession number AF 357240) was detected with a pair of primers, TACCCTAGTGGATCTGGCAAAGAC (position 1416) and GAACCCGGATAACGCTGATTAGA (position 1808), which gave a PCR product of 415 bp. $SK3/K_{Ca}2.3$ (GenBank accession number AF 357241) was detected with a pair of primers, TCCAAGCTATCCACCAACTTCG (position 1862) and TGGGAAAGAGGTGGAGCTGAT (position 2194), which gave a PCR product of 353 bp. $SK4/K_{Ca}3.1$ (GenBank accession number NM008433) was detected with a pair of primers, AAGCTCCGGGAACAAGTGAAT (position 1112) and primer GAGCTCGGTCCTTGGGTACTTA (position 1348), which gave a PCR product of 258 bp. After amplification, PCR amplicons were labeled by ethidium bromide and separated by electrophoresis on agarose gel electrophoresis. Amplicons were of the expected size and sequence. RT-PCR was performed using procedures designed to minimize the chance of cross-contamination. Negative controls for contamination from extraneous DNA were run for every batch of neurons. Contamination from extraneous sources was checked for by eliminating the cellular template for one reverse transcript reaction. The controls were consistently negative in these experiments.

Computer simulations. Simulations were performed using NEURON 5.6 (Hines and Carnevale, 2001). All channel descriptions used were the same as used by Mercer et al. (2007), except the model SK current had its deactivation rate constant reduced by a factor of ~10, to more closely match our experimental measurements. For all simulations, an integration time step of 0.025 ms was used. For simulations of autonomous activity, 10 s were simulated, and the first 5 s of results were discarded to ensure that our analyses were performed at steady state. The original NEURON channel descriptions from Mercer et al. (2007) are available in their original context from ModelDB. A package containing the channel descriptions in their current context as well as NEURON hoc code needed to

recreate the simulations will be posted on the ModelDB website (http://senselab.med.yale.edu/modelDB).

Results

GP neurons express functional SK channels

Previous *in situ* hybridization and immunohistochemical studies have suggested that SK channels are expressed by GP neurons (Stocker and Pedarzani, 2000; Sailer et al., 2004). However, it is not known whether these channels are expressed by GABAergic GP projection neurons or in the cholinergic neurons from the basal forebrain, which are intermingled with them. To address this, we performed single-cell RT-PCR on identified GP neurons, from acute mouse slices, and profiled them for the expression of GAD67 along with PV or ENK, which are specific to GABAergic GP projection neurons (Kita, 1994; Chan et al., 2004; Mercer et al., 2007). Seventeen neurons, which were positive for the GP neuron markers, were also profiled for K_{Ca}2.1, 2.2, 2.3, and 3.1 mRNA. All neurons expressed one of more K_{Ca}2 mRNA. These ion channels are commonly known as SK1, 2, and 3 and the non-neuronal SK4 channel, respectively. We found that individual GP neurons mainly express mRNA for K_{Ca}2.1 and K_{Ca}2.3, and to a lesser extent, K_{Ca}2.2 (Fig. 1*A*).

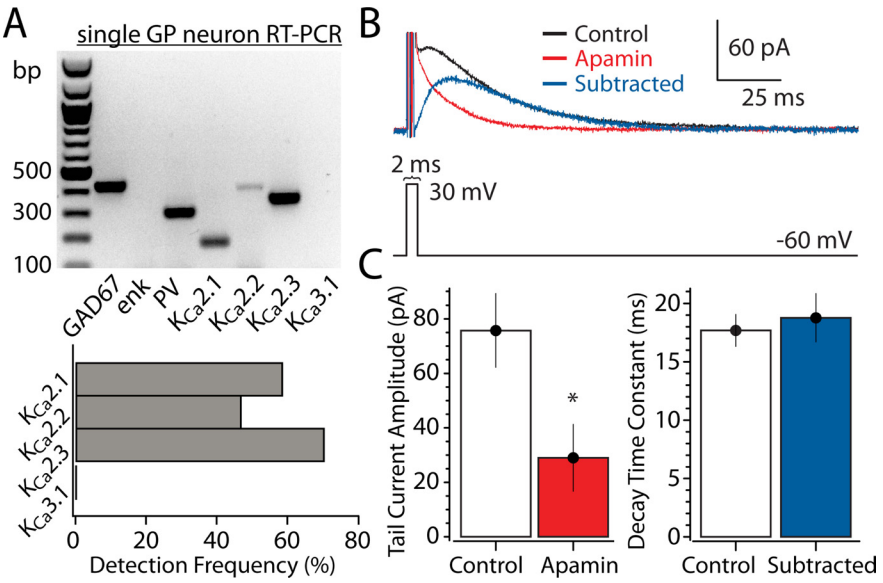

Figure 1. GP neurons express functional SK channels, which contribute to the medium afterhyperpolarization. ***A***, Example gel showing RT-PCR amplicons for both GAD67 and PV, which were used as markers for GP projection neurons. The neuron in this example coexpressed K_{Ca}2.1, 2.2, and 2.3. Below that is a summarized detection bar chart for the sample of 17 neurons. The non-neuronal K_{Ca}3.1 was never detected. ***B***, Voltage-clamp measurement of the SK current in rat GP cells in slices. The currents that underlie the afterhyperpolarization were elicited by applying a 1–2 ms voltage pulse to 30 mV from a holding potential of −60 mV. Example sets of currents are shown for control ACSF (black), 100 nM apamin (red), and the apamin-sensitive current (blue) obtained by subtracting the current recorded in apamin from the control current. ***C***, Sample measurements of peak amplitudes and decay time constants from a sample of four neurons recorded in perforated-patch configuration and two neurons recorded in the whole-cell configuration. Asterisk denotes a statistically significant change.

To determine whether SK channels are expressed and contribute to the action potential AHP, we made whole-cell and gramicidin-based perforated-patch recordings from visualized rat GP neurons. Neurons were selected for recording based on apparent health, which was determined by having a low-contrast image under IR-DIC visualization and the presence of spontaneous action potential generation. Most recordings were from neurons in the central portion of the GP and not the striatal–GP border. GP neurons were held at −60 mV using the voltage-clamp technique, and brief (1–2 ms) voltage pulses were applied. During these brief pulses, the neurons escaped the voltage clamp, and a single action current was triggered. Upon termination of the pulse, the voltage clamp was restored, and the outward currents that underlie the mAHP were revealed (Fig. 1*B*). These currents did not include the large and fast component of the AHP responsible for action potential repolarization, which was obscured by the capacitive transients that follows the pulse. Bath application of 100 nM apamin, a selective SK channel antagonist, led to a significant reduction of the AHP current amplitude from an average of 75.7 ± 13.5 pA in control to 29.0 ± 12.3 pA in apamin ($p < 0.05$, Wilcoxon signed-rank test, $V = 21$; $n = 6$) as measured from the peak of the control current (Fig. 1*C*). To determine the time course of the SK current, we subtracted the currents recorded in apamin from those recorded in control solutions (Fig. 1*B*). We found the average decay time constant to be 18.8 ± 2.1 ms ($n = 6$) for the apamin sensitive current; this was not significantly different from controls, which averaged 17.7 ± 1.4 ms. These results show that SK channels are the main determinant of the mAHP.

The SK current's contribution to the mAHP controls the precision of autonomous firing

Our voltage-clamp recordings showed that SK currents are the primary contributor to the mAHP. To test the possibility that their contribution to the mAHP also plays a role in the pattern of spontaneous action potentials, we recorded autonomous action potential discharge from visually identified GP neurons in rats and mice in either the perforated-patch or cell-attached configurations, which were chosen due to their noninvasive nature. Recordings were made in the presence of antagonists for fast synaptic transmission (see Materials and Methods) to eliminate its possible contribution to variability or any presynaptic effects induced by our drug applications. In rats, bath application of 100 nM apamin reduced the amplitude of the mAHP and consistently decreased the regularity of autonomous firing (Fig. 2*A*). The change in regularity was not due to a change in firing rate, because it was observed regardless of the direction of rate changes that occurred after apamin (Fig. 2*B*). On average, there was an approximate sixfold increase in the coefficient of variation (CV) of interspike intervals when apamin was present (control CV = 0.08 ± 0.01; apamin CV = 0.55 ± 0.16; $n = 15$), which was statistically significant ($p < 0.001$, Wilcoxon signed-rank test, $V = 1$; $n = 15$). CV was measured for 100 consecutive interspike intervals across all cells. On average apamin had no significant effect on mean firing rate (control mean frequency = 16.75 ± 3.45 Hz; apamin mean frequency = 15.94 ± 5.22 Hz; $p > 0.5$; $V = 71$; $n = 15$) (Fig. 2*C*). Examination of the membrane potential trajectory between action potentials revealed that apamin caused a reduction of the depth of the AHP and made the later ramp-like approach to firing threshold shallower (Fig. 2*A*,*B*).

In mice, bath application of 100 nM apamin also increased the amount of variability in autonomous firing (Fig. 2*D*). On average, 100 nM apamin increased the CV by twofold (control CV =

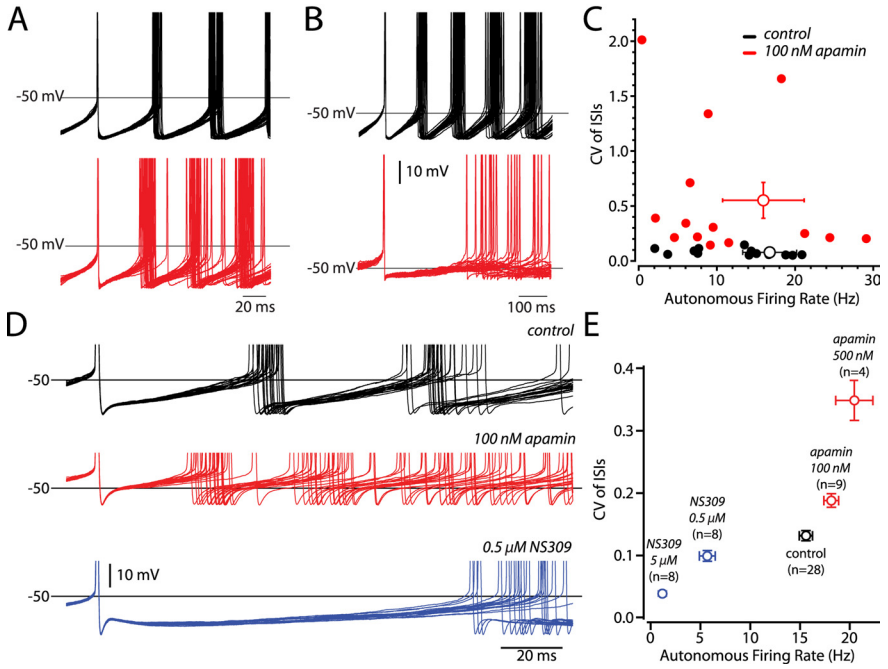

Figure 2. SK channels control the rate and enhance the regularity of spontaneous firing. ***A***, Thirty spontaneous action potentials recorded in the perforated-patch configuration, obtained from rat, are shown aligned and superimposed to show the reliability of the period of oscillation. In control solution (black traces), the action potentials repeat in a regular manner, as indicated by the relative lack of jitter in the next two periods of the oscillation. In 100 nM apamin (red traces), there is a large increase in the amount of jitter, despite the small increase in firing rate. ***B***, SK channel blockade also disrupted firing regularity when the rate was reduced after 100 nM apamin, as shown by perforated-patch recording obtained from rat. ***C***, Measurements from a sample of 15 rat neurons, showing no statistically significant change in mean firing rate, but a large and significant increase in variability of firing (indicated by the CV). Individual cells are shown as closed circles, and the average of each group is shown as an open circle. ***D***, Similar results were observed in GP neuron recordings from mouse. Action potentials are superimposed as in ***A*** for control solutions (black), 100 nM apamin (red), and 0.5 μM NS309 (blue), an SK channel agonist. Apamin application led to an increase in jitter and firing rate, corresponding to a reduction of the afterhyperpolarization both in depth and length. ***E***, Measurements from a sample of mouse GP neurons recorded in the cell-attached configuration showing a significant increase in rate and variability in apamin. NS309 application led to a significant decrease in rate and variability.

0.13 ± 0.01, $n = 28$; apamin CV = 0.20 ± 0.02; $n = 9$; $p < 0.05$, Mann–Whitney U). Application of a much larger concentration of apamin (500 nM) led to a further increase in CV, to an average of 0.35 ± 0.03 ($n = 4$; $p < 0.05$, Mann–Whitney U). In both concentrations of apamin, there was consistently a small increase in mean firing rate from 15.59 ± 0.63 Hz ($n = 28$) in control solutions to 17.12 ± 1.35 ($n = 9$; $p < 0.05$, Mann–Whitney U) in 100 nM apamin and 20.46 ± 2.16 Hz ($n = 4$; $p < 0.05$, Mann–Whitney U) in 500 nM apamin (Fig. 2*E*). Just as we observed in rat GP neurons, apamin reduced mAHP depth and made the ramp shallower (Fig. 2*E*). Apamin block of SK channels is noncompetitive and resisted washout of our slice preparation, so to confirm the actions of apamin on the SK channel, we also examined the effects of the selective SK current enhancer NS309 (Pedarzani et al., 2005; Hougaard et al., 2007). NS309 does not act as an agonist by mimicking Ca^{2+}, but instead enhances the apparent affinity between Ca^{2+} and the SK channel complex (Strøbæk et al., 2004). Bath application of NS309 caused a large increase in mAHP size, decreased the variability of autonomous discharge, and decreased the mean firing rate (Fig. 2*D*). These effects were dose dependent, and both 0.5 and 5 μM NS309 caused a significant decrease in CV and mean firing rate (CV = 0.11 ± 0.02, mean firing rate = 5.86 ± 0.76 Hz; $n = 8$; $p < 0.05$, Mann–Whitney U in 0.5 μM; and CV = 0.04 ± 0.004, mean firing rate = 1.17 ± 0.16; $n = 8$; $p < 0.05$, Mann–Whitney U in 5 μM) (Fig. 2*E*). These results demonstrate that SK channels are an important part of the pacemaking mechanism of GP neurons, with profound influence on the precision of autonomous discharge and with secondary effects on its rate.

In vitro, in the absence of all synaptic inputs, GP neurons fire rhythmically at rates between 10 and 20 Hz. However, *in vivo* GP neurons are reported to fire at much higher rates, typically 25–40 Hz for rodents and 50–80 Hz for primates (DeLong, 1971; Kita and Kitai, 1991; Sachdev et al., 1991; Gardiner and Kitai, 1992). With a decay time constant of ~20 ms, the SK current triggered by single action potentials at such high rates might accumulate and act more like a constant K^+ current, and so have no influence on regularity of firing. We addressed this by making perforated-patch recordings from rat GP neurons and applied 800 ms current injections from −80 to 140 pA, to control firing rate in a stepwise manner. An example response to a 40 pA current injection can be seen in Figure 3*A*. Both the CV and rate of firing were increased in apamin (100 nM), and the effects of apamin on regularity of firing were larger with increased current and higher firing rate. We made plots of mean frequency against injected current amplitude (FI plot) for each neuron. The average FI plot for eight neurons is shown in Figure 3*B*. Apamin caused a small but significant increase in the population FI relationship (main drug effect: $p < 0.05$; interaction: $p > 0.5$; two-way repeated-measures ANOVA; $n = 8$) (Fig. 3*B*). We also constructed plots of CV against current injection (CV–*I* plot), and apamin caused a significant increase in the CV–*I* relationship (main drug effect: $p < 0.01$; interaction: $p > 0.5$; two-way repeated-measures ANOVA; $n = 8$). These results show that the contribution of SK currents to the firing pattern of GP neurons increases with firing rate, and so can also be expected to have a substantial impact on spike timing, even at rates observed *in vivo*.

SK channels govern the availability of subthreshold voltage-gated ion channels and minimize spike threshold variability

Our results show that SK channels have a critical role in maintaining the precision of the GP neuron's intrinsic firing pattern. This influence is present even at resting rates, at which the SK current dissipates early in the interspike interval, and is long over at the time of the next action potential. This suggests that SK channels activated early in the interspike interval somehow coordinate other pacemaking currents that are active later. Perhaps the effect on regularity of firing is exerted by controlling availability of the persistent Na^+ current. Availability of Na^+ current is known to regulate the regularity of firing, as partial blockade of Na^+ channels in GP neurons leads to a loss of precision in autonomous discharge (Mercer et al., 2007). The availability of Na^+ channels is strongly regulated by the mAHP because the hyperpolarization it provides enhances recovery from inactivation and increases the number of available channels (Patlak, 1991; Vervaeke et al., 2006).

Decreased Na^+ channel availability, without any counteracting change in other subthreshold-activated currents, will result in a depolarization in spike threshold. Spike threshold was determined by constructing phase plots of dV_m/dt against V_m and noting where the rate of change in the graph was greatest, just preceding an action potential (Fig. 4*B*). In our sample of spontaneous activity recorded from rat neurons using the perforated patch configuration, apamin did cause a small, but statistically significant, depolarization of the spike threshold for spontaneously generated action potentials (Fig. 4*C*). The average value of spike threshold was -40.47 ± 2.79 mV in control solutions and -36.59 ± 3.42 mV in apamin ($p < 0.05$, Wilcoxon signed-rank test, $V = 10$; $n = 11$). Apamin also significantly increased the variability in spike threshold (Fig. 4*A*,*B*), measured as the SD in spike thresholds of 100 consecutive spikes across neurons. In control conditions, the SD was on average 0.92 ± 0.11 mV and increased to 1.12 ± 0.13 in apamin ($p < 0.05$, Wilcoxon signed-rank test, $V = 9$; $n = 11$). As can be seen in the example in Figure 4*B*, apamin did not significantly reduce the maximal slope of the rising phase of the action potential, max dV_m/dt (control mean = 132.19 ± 18.16 mV/ms; apamin mean = 127.81 ± 23.44 mV/ms; $p > 0.5$, Wilcoxon signed-rank test, $V = 34$, $n = 11$), which is sometimes also used as a measure of spike-generating, or transient, Na^+ channel availability (Weidmann, 1955; Gettes and Reuter, 1974; Colbert et al., 1997). Because spike threshold depolarization did not coincide with a decrease in max dV_m/dt, it is likely that apamin causes downstream effects on currents that determine threshold, such as persistent Na^+ or subthreshold K^+ currents—but not transient spike-generating Na^+ current exclusively.

SK channel blockade leads to a small depolarization in spike threshold as well as an increase in spike threshold variability, but a reduction in Na^+ channels alone cannot account for apamin's effect on threshold. Furthermore, a reduction in Na^+ channel availability alone should cause a dramatic reduction in rate (Mercer et al., 2007), whereas apamin causes either no change in rate or a small increase. One possibility is that another current functionally opposed to the persistent Na^+ current is also inactivated, such as an A-type K^+ current. In other rhythmically firing neurons, transient K^+ currents are activated during a pacemaking cycle around spike threshold (Jackson and

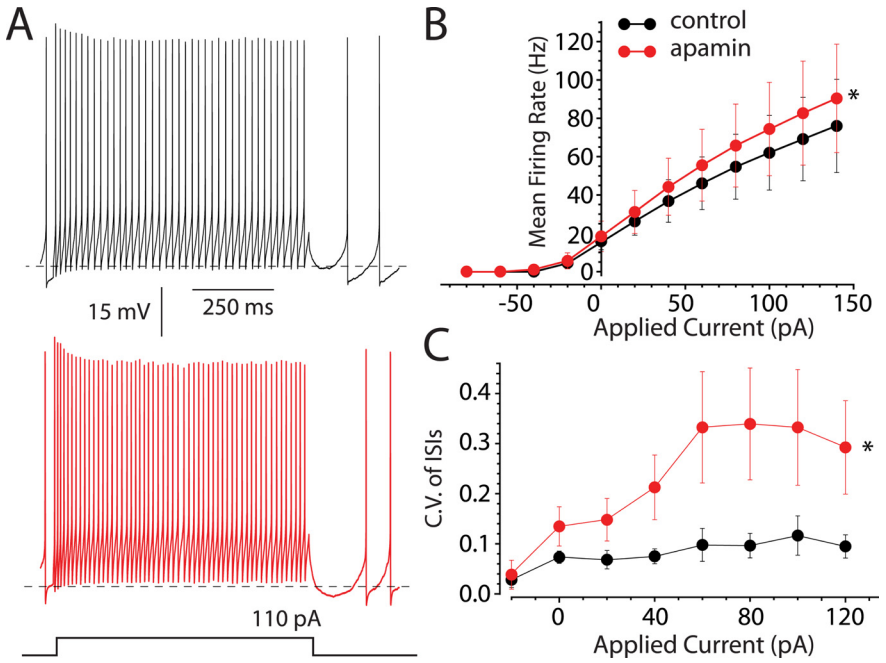

Figure 3. SK channels help to determine the rate and regularity of externally driven repetitive firing. ***A***, Rat GP neurons recorded in the perforated-patch configuration were given current injections in a stepwise manner. The traces depicted show the response to a single current step to 40 pA in control ACSF (black trace) and in apamin (red trace). ***B***, Plot of frequency versus applied current (*F–I* plot) for a sample of nine neurons. The asterisk denotes a significant change in the plot. ***C***, Plot of firing irregularity versus applied current (CV–*I* plot) for a sample of nine neurons. The asterisk denotes a significant change in the plot.

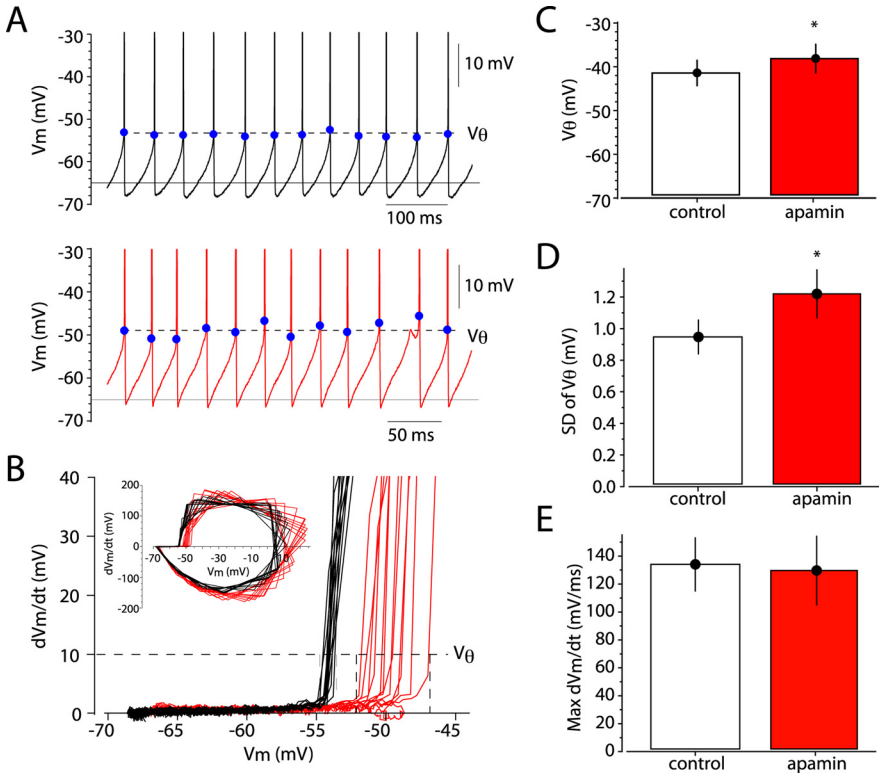

Figure 4. SK channels determine spike threshold and minimize spike threshold variability. ***A***, Example voltage traces from a rat neuron recorded in the perforated-patch configuration before (black) and after 100 nM apamin (red); threshold is indicated by blue dots. Spikes are truncated here to emphasize the location of spike threshold (V_θ). ***B***, Phase plots of dV_m/dt against membrane voltage. These plots show the variability in threshold and where threshold was defined. ***C***, Apamin effect on V_θ for our sample. ***D***, Apamin effect on the SD in V_θ for our sample. ***E***, Apamin effect on the maximal rate of rise for action potentials (max dV_m/dt) for our sample. Asterisk denotes statistically significant change.

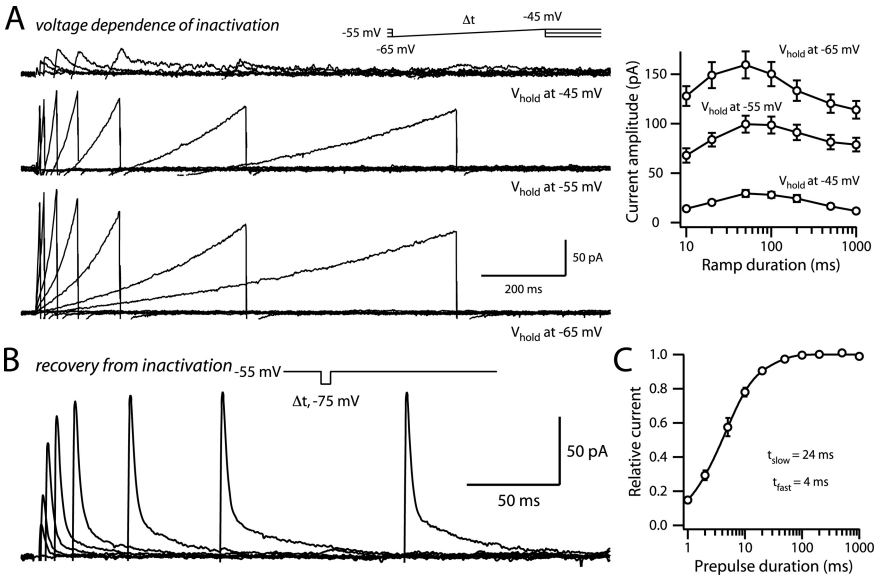

Figure 5. An inactivating K^+ current makes the largest outward current contribution during pacemaking. ***A***, Outward currents evoked in the whole-cell configuration, in mouse GP neurons, using a ramp-shaped protocol (inset) that consisted of holding at a potential of −65, −55, or −45 mV and then ramping the voltage from −65 to −45 mV. The duration of the ramp (Δt) was also varied. Example currents evoked using this protocol are shown for each holding potential, and summary data are plotted as a function of ramp duration. ***B***, The rate of recovery was assessed by applying a hyperpolarizing step to −75 mV for a variable period of time (Δt) from a holding potential of −55 mV and then stepping back to the holding potential. This small subthreshold step from −75 to −55 mV was enough to evoke a substantial amount of current. ***C***, Relative current evoked in ***B*** for our sample, plotted as a function of time. This relationship was described best with a sum of two exponentials; the fast time constant in this example was 4 ms, and the slower one was 24 ms.

Bean, 2007; Khaliq and Bean, 2008). Inactivation of these currents may also affect spike threshold in a direction opposite to that of the persistent Na^+ current. GP neurons are known to express inactivating K_v4 family subunit-mediated A-type K^+ currents, whose voltage properties are very similar to the persistent Na^+ current (Tkatch et al., 2000).

The A-type K^+ current's participation in the pacemaking of GP neurons is difficult to demonstrate in current clamp, because of their pharmacological overlap with K_v3-containing delayed rectifiers. We used voltage clamp to confirm that inactivating currents could be evoked with subthreshold depolarization like those during pacemaking as predicted by their activation properties (Tkatch et al., 2000). To mimic the voltage trajectory during a cycle of pacemaking, we made whole-cell recordings from mouse GP neurons and applied voltage ramps that spanned the subthreshold range (−65 mV to −45 mV). We varied the starting potential of the ramp, which was −65, −55, or −45 mV, to approximate the observed AHP depths under different levels of SK activation, as in Figure 2. We also varied the ramp duration to determine the effects of voltage trajectory. To isolate the outward component of the subthreshold evoked current, we included 1 μM TTX to block inward Na^+ currents. The outward current evoked by the ramp was sensitive to the starting potential, suggesting that the dominant K^+ current activated during pacemaking is an inactivating K^+ current (Fig. 5*A*). To ensure that a sufficient amount of current could be recovered by a short duration hyperpolarizing as occurs during the mAHP, we held neurons at a potential of −55 mV, allowing for a steady-state level of inactivation, and then stepped to −75 mV for a variable period of time and then back to the holding potential (Fig. 5*B*,*C*). The small step from −75 back to −55 mV was enough to evoke a substantial amount of current even when the duration was as short as 10 ms. These transient currents are consistent with A-type K^+ currents (Tkatch et al., 2000), and fast enough for the mAHP to affect recovery in a substantial way. These results show that the inactivating K^+ currents contribute the majority of the outward current during pacemaking and, in a manner similar to Na^+ current, are active just before threshold. Thus both the persistent Na^+ current and the inactivating K^+ current, which are responsible for pacemaking, are dependent on the mAHP for recovery from inactivation during an action potential.

Simulations of the SK channel's contribution to voltage-gated ion channel availability and precision of firing

We hypothesize that both of the two major subthreshold voltage-activated currents, with opposing roles during the interspike interval, are reduced after SK channel blockade. How the reduced availability of these currents underlies the loss of precision and variability in threshold is difficult to directly address using only experimental techniques. We made use of numerical simulations to determine how the interaction between SK and these subthreshold voltage-gated ion channels determines the precision of firing. The model we used was a single compartment reduction of that used by Mercer et al. (2007), except that the model of the SK channel model's deactivation rate constant was reduced by a factor of ~10. The model contained multistate Markov models of the GP neuron's known voltage-gated ion channels, which consisted in particular of voltage-gated Na^+ channels $Na_v1.1/1.2$ and $Na_v1.6$ (Na_v) as well as the A-type K^+ channel $K_v4.2/4.3$ (K_v4). Despite the reduction of the model to a single compartment, it was able to fire autonomously with similar voltage trajectories as our recordings. Simulations were implemented in NEURON (Hines and Carnevale, 2001). The mean firing rate was 23–24 Hz, which is slightly higher than the original multicompartment model, but still within the natural range of autonomous GP cell firing rates in slices. The Mercer et al. (2007) model did not include a source of variability in interspike intervals, and the origin of variability in GP neurons is not known. We included variability in the model by adding a nonspecific leak channel whose maximal conductance was scaled at each integration step by an amount drawn at random from a normal distribution with a mean of 0 and an SD of 0.001, so the mean current was always zero during the interspike interval. The reversal potential of this noisy conductance was −70 mV. A detailed description of all channels present, their properties and densities are available as supplemental material (available at www.jneurosci.org).

When SK current is removed in this simple model, the rate of spontaneous firing increases from 24.0 to 32.5 Hz; in the experiments, apamin produced little to no effect on mean spontaneous firing rate, depending on the species. We set out to explain why this was true of our model in an attempt to understand the heterogeneity of rate effects seen in apamin (Figs. 2, 3). If SK current's effect on rate and precision are actually mediated by controlling the relative availability between Na_v and K_v4 currents, then by altering the maximum availability of either Na_v or K_v4

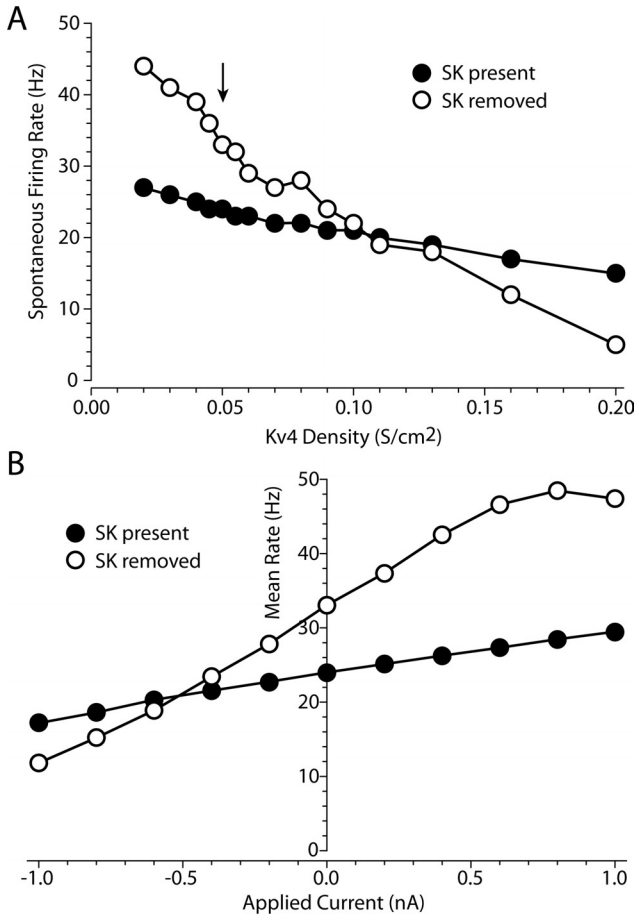

Figure 6. The initial availability of Kv4 current determines the effect of SK current removal on firing rate. ***A***, The density of Kv4 channels was varied over a 10-fold range from 0.02 to 0.2 S/cm^2, while the density of all other currents were fixed. The rate of spontaneous firing was measured over this range before (black circles) and after the removal of SK current (open circles). The black arrow indicates the value of Kv4 (0.05 S/cm^2) used in our model. ***B***, The relationship between frequency and applied current in our model using the Kv4 density value indicated by the arrow in ***A***.

current relative to the other, we may see SK current's influence on rate is context dependent. For example, if SK channel block leads to an equal reduction in both currents, there will be no change in rate. But if there were more K_v4 channels available, blocking SK would have a larger effect on Na_v current than K_v4, and the net effect would be a decrease in rate. Even among relatively homogenous populations of neurons, the total number of ion channels of a given species, such as $K_v4.3$, can vary over a wide range, leading to heterogeneity in various aspects of pacemaking, such as rate (Liss et al., 2001). This kind of variability in the total availability of ion channels may also account for the natural variability observed among GP neurons recorded in slices (Günay et al., 2008). We ran a series of simulations in which we kept the density of Na_v fixed at their starting values (0.2 and 0.12 S/cm^2 for Nav1.1/2 and 1.6, respectively) and varied the density of K_v4 current over a 10-fold range (0.02–0.2 S/cm^2). For each simulation, we measured the average rate of spontaneous firing before and after the removal of SK current. Removing SK current led to an increase in firing rate when the density of K_v4 was <0.1 S/cm^2 (Fig. 6*A*). Our initially chosen value of 0.05 S/cm^2 is in this range. At a density value of $\sim$0.11 S/cm^2, there is no change in firing rate accompanying the removal of SK current. Beyond values of 0.11 S/cm^2 and up to our maximum density of 0.2 S/cm^2, removing SK current resulted in a decreased firing rate (Fig. 6*A*). Thus, the density of K_v4 relative to Na_v channels will determine how the rate of spontaneous firing will be altered after the removal of SK current. In our experiments, as we increased the GP neuron's firing rate by applying depolarizing current injections, we observed consistent increases in firing rate after SK channel blockade (Fig. 3). We found a similar relationship between applied current and frequency in our model, except that for our chosen value of K_v4 there is an increase in the spontaneous firing rate after the removal of SK. When the rate is slowed down by hyperpolarizing current injections, the point at which there is no net effect on rate can be seen (Fig. 6*B*). Beyond this point, removing SK current results in a decreased firing rate, because the influence of SK on Na^+ channel inactivation dominates.

Because in our experiments, we saw that there was a decrease in the precision of pacemaking regardless of whether apamin influenced the firing rate, we choose to pursue the mechanism of decreased precision in our model despite the increase in firing rate accompanying SK current removal. When SK channels were present, the CV of interspike intervals was 0.08 and the SD in spike threshold was 0.96 mV. When SK channels were removed both the CV of interspike intervals and the variance in threshold increased to 0.33 and 1.88 mV, respectively (Fig. 7*A*). The addition of the noisy conductance was thus sufficient to produce both the variation of interspike intervals and variation of thresholds seen in our experiments, as well as the effects of apamin on both forms of variability. Similar results were obtained when we matched the firing rates by applying a hyperpolarizing current injection to the model after the removal of SK channels (data not shown). The model was analyzed to determine the mechanisms responsible for these effects. We made phase plots of fractional channel availability as a function of membrane voltage for 1 s of simulated autonomous activity (Fig. 7*B*). These plots were constructed from the simulations depicted in Figure 7*A* and they evolve in a clockwise manner; availability is defined as the proportion of noninactivated channels. Availability of both channels reached its maximum level during the mAHP. Although total inward and outward current were nearly balanced throughout the depolarizing phase of the interspike interval, availability of Na_v channels was maintained during the approach to threshold, whereas K_v4 availability gradually decreased. Na_v availability dropped during the falling phase of the action potential and recovered during the mAHP. The effect of the added noisy conductance can be seen in the availability plots and occurs in a voltage window (approximately -60 to -50 mV) corresponding to the ramp-like part of the interspike membrane potential trajectory. The maximal availability of both K_v4 and Na_v channels were greatly reduced when SK channels were removed, and the noise caused variability in channel availability. There was little or no change in threshold even though Na_v channel availability was clearly reduced, because there was a matched of reduction in K_v4.

The mechanism that underlies the neuron's increased noise sensitivity after removal of SK current is related to the large reduction of K_v4 and Na_v currents. However, because we see an increase in the noise sensitivity regardless of how the neuron's firing rate changes, it may not be the result of how the availabilities of Na_v or K_v4 change relative to each other, but instead a general reduction in their availability. This could arise simply by the reduction in Na_v and K_v4 current causing an increase in the neuron's input resistance. Because the decrease in channel availability occurs regardless of firing rate change, this mechanism can influence precision independently of rate. To test this, we calculated the instantaneous current–voltage relationship at points

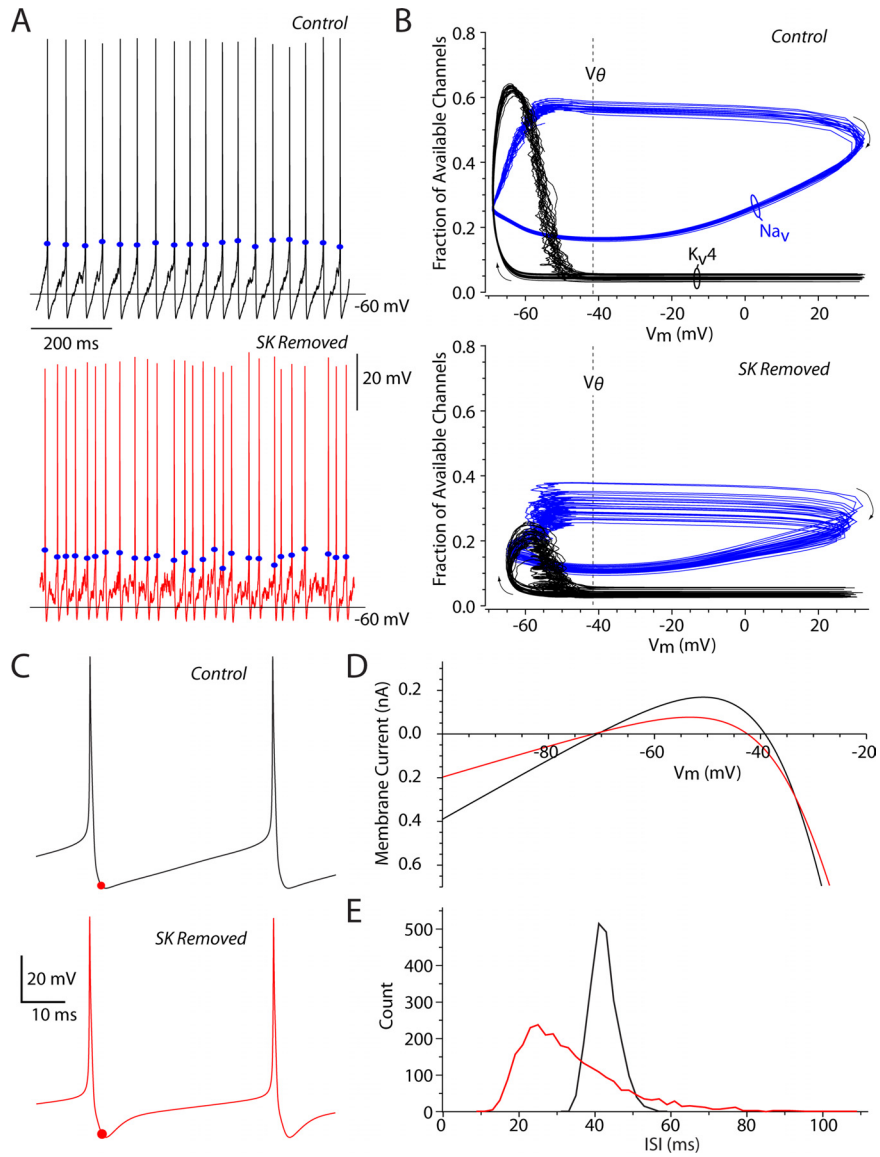

Figure 7. Simulations of SK channel's effect on subthreshold voltage-activated ion channel availability and neuronal noise sensitivity. ***A***, Example voltage traces from simulated autonomous activity both when SK is present (control, black) and when SK is removed (red trace). Blue dots indicate spike threshold. ***B***, Phase plots of fractional channel availability for both voltage-gated Na^+ (Na_v, blue) and A-type K^+ (K_v4, black). These plots evolve in a clockwise manner and show how availability changes during a spike. Vertical dashed line indicates location of spike threshold (V_θ). ***C***, The same model in the absence of noise was used to simulate autonomous activity before (black) and after the removal of SK channels (red). The red dot indicates the point at which all channel variables were frozen. ***D***, Instantaneous *I–V* curve made by allowing the Na_v activation to vary instantaneously while all other gating variables were frozen in ***C***. ***E***, Interspike interval (ISI) histogram generated by applying noisy current injections to the neuron and counting an equal number of spikes before (black) and after (red) the removal of SK.

throughout the interspike interval. An example showing the instantaneous *I–V* relationship of similar points during an interspike interval before and after the removal of SK is shown in Figure 7*C*. In Figure 7*C* the noisy conductance has been removed to allow calculation of the *I–V* relationship. The removal of the noisy conductance abolished the difference in firing rate after SK current removal. This was because the balanced point between K_v4 and Na_v reduction, as shown in Figure 6*C*, shifts to the left when noise is absent, and in our example moved to the density value of our model (data not shown). To construct the instantaneous *I–V* curve at the indicated points, we determined the values of all gating variables of the model at this point and froze them, but because we want to know how the membrane will respond to relatively fast changes in voltage, we allow the fastest variable in the model to change instantaneously—this is the activation of Na_v. Current contributed by all ion channels in the model was calculated across a wide voltage range of −120 to 40 mV, and finally the total sum of these ionic currents was plotted against voltage (Fig. 7*D*). The slope of this curve at any given point is the neuron's slope conductance, which is inversely proportional to the input resistance. The instantaneous *I–V* curves maintained a similar shape throughout the depolarizing phase of the interspike interval, but slowly drifted downward as the cell approached spike threshold. They exhibited a pair of zero-current points that approach each other as the neuron approached threshold. The voltage corresponding to the action potential threshold corresponds to the maximum of the instantaneous *I–V* curve. The effect of matched inactivation of the inward and outward currents was a reduction of the slope conductance at the left zero-current point, with little or no change in the maximum value. Current noise produced small vertical excursions of the entire curve, which resulted in action potentials when larger than the distance between the zero-crossing and the peak of the *I–V* curve. Reduction in the slope conductance caused by accumulated inactivation of both Na_v and K_v channels after removal of the mAHP decreased this distance, resulting in increased sensitivity to noise and apparent changes in the threshold voltage. The effect of the change in slope conductance on the interspike interval histogram for the model neuron is shown in Figure 7*E*.

Discussion

Spike-triggered afterhyperpolarization currents are key elements in the mechanism of oscillation of globus pallidus neurons. Over most of the voltage range visited during the interspike interval, the steady state *I–V* curve of GP cell is dominated by a negative slope conductance created by the persistent Na^+ current (Chan et al., 2004; Mercer et al., 2007). After an action potential, hyperpolarization-activated HCN current returns the membrane potentials to the activation range of the persistent Na_v current, which then ensures a gradual depolarization of the cell until the next action potential is triggered (Chan et al., 2004). The balance of subthreshold-activated Na^+ and K^+ currents determines the rate of depolarization during the interspike interval membrane potential trajectory. The ratio of these currents is approximately constant over most of the interspike interval, as indicated by the approximately linear ramp-shaped depolarization between action potentials (Schwindt and Calvin, 1972). The interspike interval of the autonomous oscillation is determined by the depth

of the afterhyperpolarization (which determines the total voltage excursion between action potentials), the duration of the afterhyperpolarization current (which delays the onset of the ramp-like depolarization), and the size of the net inward current that brings the cell to threshold. AHP currents unquestionably control the first two of these, and may influence the third. Calcium-dependent afterhyperpolarization currents from SK channels have the additional property of voltage independence, making their strength and duration relatively independent of synaptic input and intrinsic noise. Thus they are well suited to stabilize the membrane potential at a consistent starting point for the recovery of both voltage-gated Na^+ and transient K^+ current after each action potential, and to render the cell insensitive to current perturbations during the first part of the interspike interval.

Our modeling results show that the variety of effects SK current blockade has on the firing rate of GP neurons is at least in part the result of variations in the initial densities of the voltage-gated ion channels. However, the brief nature of the SK conductance and the presence of a strong fast AHP current in GP cells may also have some influence. SK current decayed rapidly after each action potential, and was dissipated within the first third of the interspike interval (~20 ms), so that it does not greatly delay the depolarization produced by the other voltage-sensitive currents responsible for generating reliable pacemaking. GP neurons possess a powerful fast AHP, primarily the result of voltage-gated K_v3 family ion channels (Hernández-Pineda et al., 1999, Baranauskas et al., 1999). The fast AHP of GP neurons has a strong influence over firing rate, and is able to consistently control the starting point of the interspike membrane potential trajectory, even in the absence of a mAHP. Our results suggest that the main influence of the SK current is exerted by a different mechanism, by resetting the availability of subthreshold-activated voltage sensitive currents rather than the membrane potential. In so doing, its effects extend long beyond the relatively short duration of the mAHP current. Because the total AHP current is brief, the interspike interval is primarily determined by the balance between inward and outward voltage-dependent currents acting throughout the interspike interval. These voltage-dependent currents are both inactivating, and the SK current functions primarily to promote their recovery from inactivation after an action potential. Because the SK current similarly affects them, its blockade does not greatly alter the balance between these currents, but rather their absolute amplitudes. Thus it has a small effect on oscillation period or on action potential threshold, but rather acts to control the sensitivity of the membrane potential trajectory (and firing time) to intrinsic and synaptic current perturbations.

Intrinsic variability in oscillating GP neurons is critical for determining the degree to which the cells may be synchronized by shared synaptic input. Synaptic inputs, whether excitatory or inhibitory, act to decrease the differences in phase among a collection of oscillating neurons with similar frequencies [Nakao et al. (2005), Danzl et al. (2008), and Ermentrout et al. (2008)]. This tendency of synaptic input to synchronize firing in groups of neurons sharing common inputs may be an important mechanism for the encoding of information by networks of oscillating cells. The duration of action of a synchronizing input is determined by the variability of the neurons, both in their natural frequencies and in the irregularity of their oscillations. Even for identical neurons, the influence of common input will decay at a rate determined by the degree of interspike interval irregularity. Highly irregular neurons are resistant to accumulating synchronizing influences of common inputs and mutual synaptic connections, and this may play a part in maintaining asynchronous firing in the healthy GP (Nini et al., 1995; Raz et al., 2000; Levy et al., 2002).

Intrinsic variability not only controls the decay of synchronization after a stimulus, but also the sensitivity of the cells to such stimuli. This is because the mechanisms controlling the sensitivity of the oscillation to intrinsic noise also determine the sensitivity of individual cells to synaptic inputs. A decrease in the instantaneous slope conductance during the interspike interval increases the degree to which an intervening excitatory or inhibitory input can change the timing of the next action potential. Any increase in sensitivity to synaptic inputs by this mechanism will be associated with an increased variability of the intrinsic oscillation, and resulting shortening of the lifetime of input-induced synchrony.

If the intrinsic rhythms of globus pallidus neurons form the basis for encoding synaptic input by changes in spike timing, it might be useful for the network to have a mechanism for regulating the sensitivity of the neurons to small synaptic inputs and for determining the duration of stimulus induced synchrony. The SK current is well suited to this role. Its influence is controlled by modulation of spike-triggered calcium currents, which can themselves be modulated by neurotransmitters, including dopamine (Ramanathan et al., 2008). When the SK current is strong, the periodicity of oscillatory cycle of the GP neuron will be enhanced and the sensitivity to synaptic input reduced, but the duration of synchronization generated by strong inputs will be increased. When the SK mAHP is reduced, GP cells action potentials may be less precisely timed, the sensitivity to synaptic input increased, and the lifetime of network synchrony following an input reduced.

References

Baranauskas G, Tkatch T, Surmeier DJ (1999) Delayed rectifier currents in rat globus pallidus neurons are attributable to Kv2.1 and Kv3.1/3.2 K^+ channels. J Neurosci 19:6394–6404.

Chan CS, Shigemoto R, Mercer JN, Surmeier DJ (2004) HCN2 and HCN1 channels govern the regularity of autonomous pacemaking and synaptic resetting in globus pallidus neurons. J Neurosci 24:9921–9932.

Colbert CM, Magee JC, Hoffman DA, Johnston D (1997) Slow recovery from inactivation of Na^+ channels underlies the activity-dependent attenuation of dendritic action potentials in hippocampal CA1 pyramidal neurons. J Neurosci 17:6512–6521.

Danzl P, Hansen R, Bonnet G, Moehlis J (2008) Partial phase synchronization of neural populations due to random Poisson inputs. J Comput Neurosci 25:141–157.

DeLong MR (1971) Activity of pallidal neurons during movement. J Neurophysiol 34:414–427.

Ermentrout GB, Galán RF, Urban NN (2008) Reliability, synchrony and noise. Trends Neurosci 31:428–434.

Gardiner TW, Kitai ST (1992) Single-unit activity in the globus pallidus and neostriatum of the rat during performance of a trained head movement. Exp Brain Res 88:517–530.

Gettes LS, Reuter H (1974) Slow recovery from inactivation of inward currents in mammalian myocardial fibres. J Physiol 240:703–724.

Günay C, Edgerton JR, Jaeger D (2008) Channel density distributions explain spiking variability in the globus pallidus: a combined physiology and computer simulation database approach. J Neurosci 28:7476–7491.

Hashimoto K, Kita H (2006) Slow oscillatory activity of rat globus pallidus neurons in vitro. Eur J Neurosci 23:443–453.

Hernández-Pineda R, Chow A, Amarillo Y, Moreno H, Saganich M, Vega-Saenz de Miera EC, Hernández-Cruz A, Rudy B (1999) Kv3.1-Kv3.2 channels underlie a high-voltage-activating component of the delayed rectifier K+ current in projecting neurons from the globus pallidus. J Neurophysiol 82:1512–1528.

Hines ML, Carnevale NT (2001) NEURON: a tool for neuroscientists. Neuroscientist 7:123–135.

Hougaard C, Eriksen BL, Jørgensen S, Johansen TH, Dyhring T, Madsen LS,

Strøbæk D, Christophersen P (2007) Selective positive modulation of the SK3 and SK2 subtypes of small conductance Ca2+-activated K+ channels. Br J Pharmacol 151:655–665.

Ishii TM, Maylie J, Adelman JP (1997) Determinants of apamin and d-tubocurarine block in SK potassium channels. J Biol Chem 272:23195–23200.

Jackson AC, Bean BP (2007) State-dependent enhancement of subthreshold A-type potassium current by 4-aminopyridine in tuberomammillary nucleus neurons. J Neurosci 27:10785–10796.

Khaliq ZM, Bean BP (2008) Dynamic, nonlinear feedback regulation of slow pacemaking by A-type potassium current in ventral tegmental area neurons. J Neurosci 28:10905–10917.

Kita H (1994) Parvalbumin-immunopositive neurons in rat globus pallidus: a light and electron microscopic study. Brain Res 657:31–41.

Kita H, Kitai ST (1991) Intracellular study of rat globus pallidus neurons: membrane properties and responses to neostriatal, subthalamic and nigral stimulation. Brain Res 564:296–305.

Levy R, Hutchison WD, Lozano AM, Dostrovsky JO (2002) Synchronized neuronal discharge in the basal ganglia of parkinsonian patients is limited to oscillatory activity. J Neurosci 22:2855–2861.

Liss B, Franz O, Sewing S, Bruns R, Neuhoff H, Roeper J (2001) Tuning pacemaker frequency of individual dopaminergic neurons by Kv4.3L and KChip3.1 transcription. EMBO J 20:5715–5724.

Mercer JN, Chan CS, Tkatch T, Held J, Surmeier DJ (2007) Nav1.6 sodium channels are critical to pacemaking and fast spiking in globus pallidus neurons. J Neurosci 27:13552–13566.

Nakao H, Arai KS, Nagai K, Tsubo Y, Kuramoto Y (2005) Synchrony of limit-cycle oscillators induced by random external impulses. Phys Rev E Stat Nonlin Soft Matter Phys 72:026220.

Nini A, Feingold A, Slovin H, Bergman H (1995) Neurons in the globus pallidus do not show correlated activity in the normal monkey, but phase-locked oscillations appear in the MPTP model of parkinsonism. J Neurophysiol 74:1800–1805.

Patlak J (1991) Molecular kinetics of voltage-dependent Na+ channels. Physiol Rev 71:1047–1080.

Pedarzani P, McCutcheon JE, Rogge G, Jensen BS, Christophersen P, Hougaard C, Strøbæk D, Stocker M (2005) Specific enhancement of SK channel activity selectively potentiates the afterhyperpolarizing current I_{AHP} and modulates the firing properties of hippocampal pyramidal neurons. J Biol Chem 280:41404–41411.

Ramanathan S, Tkatch T, Atherton JF, Wilson CJ, Bevan MD (2008) D2-like dopamine receptors modulate SKCa channel function in subthalamic nucleus neurons through inhibition of Cav2.2 channels. J Neurophysiol 99:442–459.

Raz A, Vaadia E, Bergman H (2000) Firing patterns and correlations of spontaneous discharge of pallidal neurons in the normal and the tremulous 1-methyl-4-phenyl-1,2,3,6-tetrahydropyridine vervet model of parkinsonism. J Neurosci 20:8559–8571.

Sachdev RN, Gilman S, Aldridge JW (1991) Bursting properties of units in cat globus pallidus and entopeduncular nucleus: the effect of excitotoxic striatal lesions. Brain Res 549:194–204.

Sailer CA, Kaufmann WA, Marksteiner J, Knaus HG (2004) Comparative immunohistochemical distribution of three small-conductance Ca2+-activated potassium channel subunits, SK1, SK2, and SK3 in mouse brain. Mol Cell Neurosci 26:458–469.

Schwindt PC, Calvin WH (1972) Membrane-potential trajectories between spikes underlying motoneuron firing rates. J Neurophysiol 35:311–325.

Stanford IM (2003) Independent neuronal oscillators of the rat globus pallidus. J Neurophysiol 89:1713–1717.

Stocker M, Pedarzani P (2000) Differential distribution of three Ca(2+)-activated K(+) channel subunits, SK1, SK2, and SK3, in the adult rat central nervous system. Mol Cell Neurosci 15:476–493.

Strøbæk D, Teuber L, Jørgensen TD, Ahring PK, Kjær K, Hansen RS, Olesen SP, Christophersen P, Skaaning-Jensen B (2004) Activation of human IK and SK Ca2+-activated K+ channels by NS309 (6,7-dichloro-1H-indole-2,3-dione 3-oxime). Biochim Biophys Acta 1665:1–5.

Surmeier DJ, Song WJ, Yan Z (1996) Coordinated expression of dopamine receptors in neostriatal medium spiny neurons. J Neurosci 16:6579–6591.

Tkatch T, Baranauskas G, Surmeier DJ (2000) Kv4.2 mRNA abundance and A-type K^+ current amplitude are linearly related in basal ganglia and basal forebrain neurons. J Neurosci 20:579–588.

Vervaeke K, Hu H, Graham LJ, Storm JF (2006) Contrasting effects of the persistent Na+ current on neuronal excitability and spike timing. Neuron 49:257–270.

Vysokanov A, Flores-Hernandez J, Surmeier DJ (1998) mRNAs for clozapine-sensitive receptors co-localize in rat prefrontal cortex neurons. Neurosci Lett 258:179–182.

Weidmann S (1955) The effect of the cardiac membrane potential on the rapid availability of the sodium-carrying system. J Physiol 127:213–224.